Electronic Supplementary Information

Flexible nanohybrid substrates utilizing gold nanocubes/nano mica platelets with 3D lightning-rod effect for highly efficient bacterial biosensors based on surface-enhanced Raman scattering

Yan-Feng Chen, [a] Ming-Chang Lu, [a] Chia-Jung Lee, [b] Chih-Wei Chiu *[a]

[a] Department of Materials Science and Engineering, National Taiwan University of Science and Technology, Taipei 10607, Taiwan

[b] Ph.D. Program in Clinical Drug Development of Herbal Medicine, College of Pharmacy, Taipei Medical University, Taipei 11031, Taiwan

*Corresponding author:

E-mail: cwchiu@mail.ntust.edu.tw; Tel.: +886-2-2737-6521

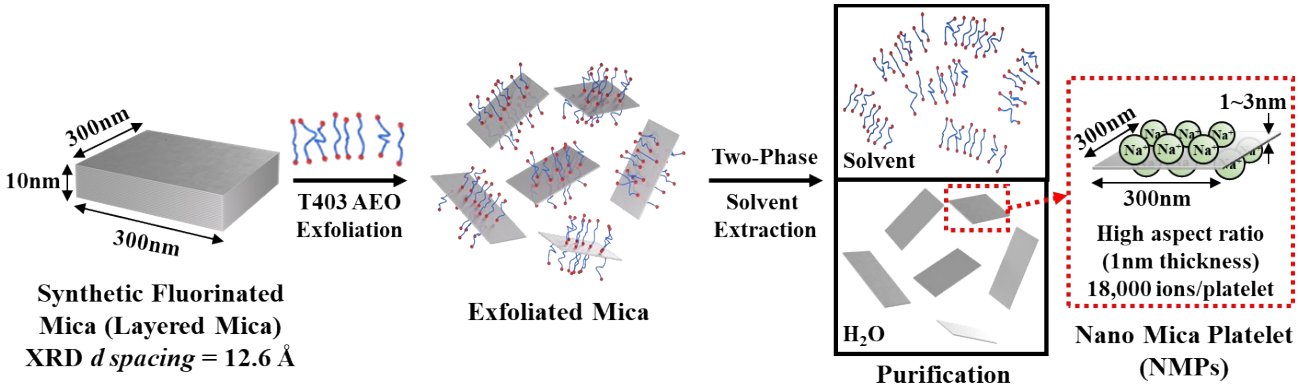

Fig. S1 Schematic of the one-step preparation of delaminated nano mica platelets (NMPs). First, the delamination agent T403AEO was used to perform a cation exchange with the clay. This process enabled NMPs to change from a layer-by-layer stacked structure to a monolithic structure. Finally, organic and inorganic extraction and filtration were used to remove surface polymers, and NMPs with a two-dimensional structure were obtained.

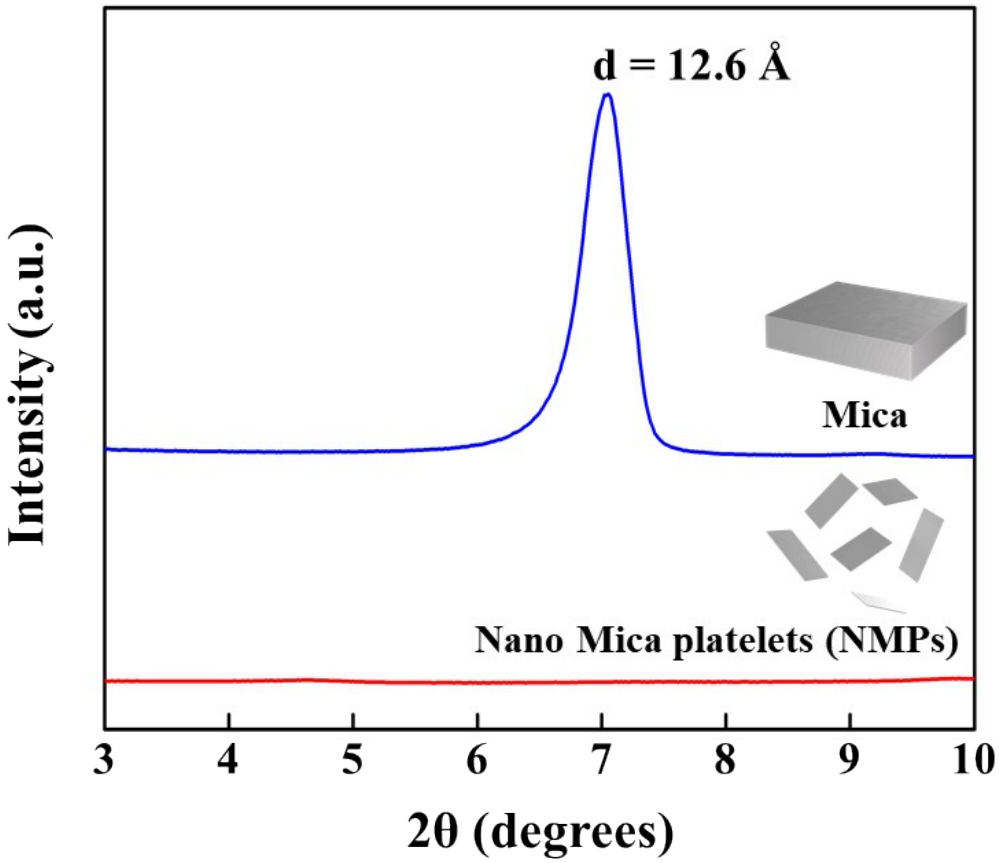

Fig. S2 X-ray diffraction patterns of Mica and NMPs, which are the layered and delaminated structures of clay, respectively.

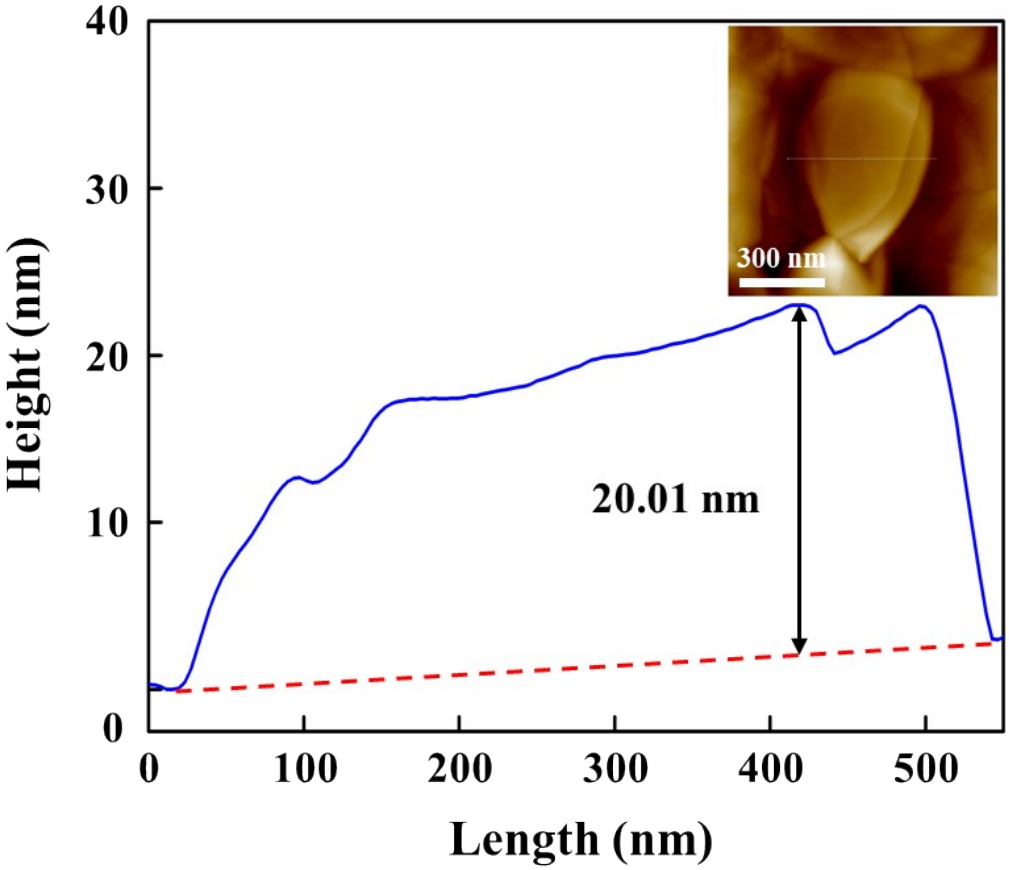

Fig. S3 Atomic force microscopy (AFM) height-distribution map of Mica in layer-by-layer stacked structure. The thickness of Mica is approximately 20.01 nm. The inset is an AFM image of pristine layered Mica without delamination. The scale bar is 300 nm.

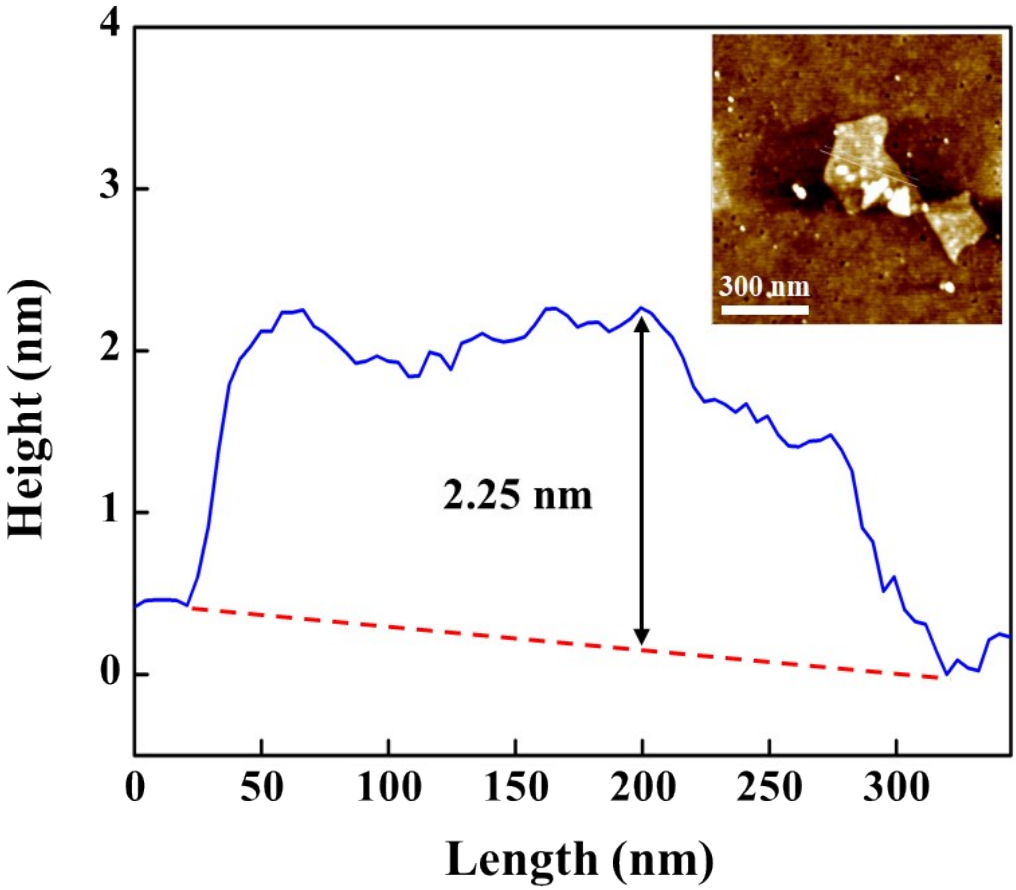

Fig. S4 AFM height-distribution map of delaminated NMPs with a thickness of approximately 2.25 nm. The inset is an AFM image of monolithic NMPs. The scale bar is 300 nm.

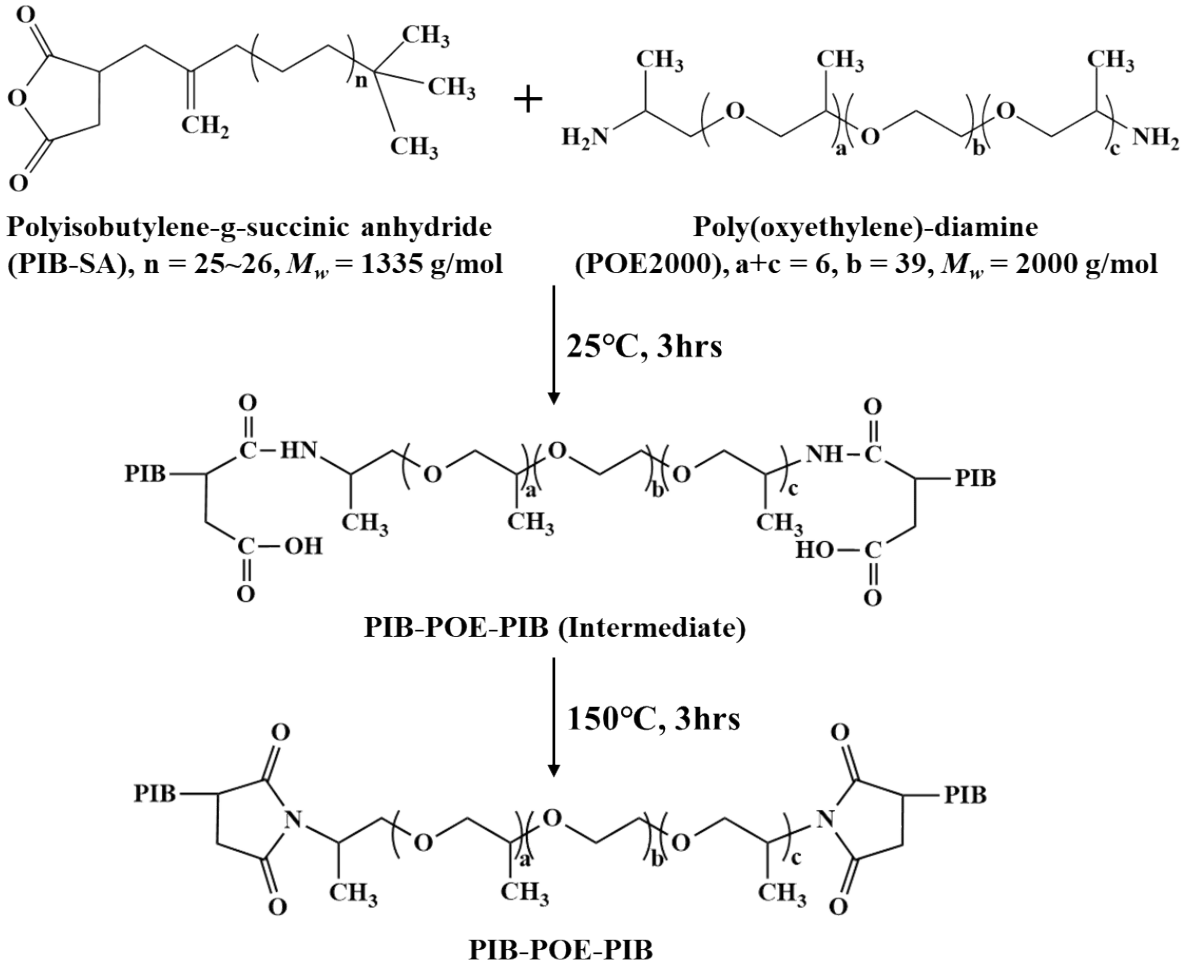

Fig. S5 Synthetic structure of the amphiphilic polymer dispersant PIB–POE–PIB, which is synthesized from Polyisobutylene-g-succinic anhydride (PIB-SA) and Poly(oxyethylene)-diamine (POE2000) through an acylation reaction and phenylation reaction.

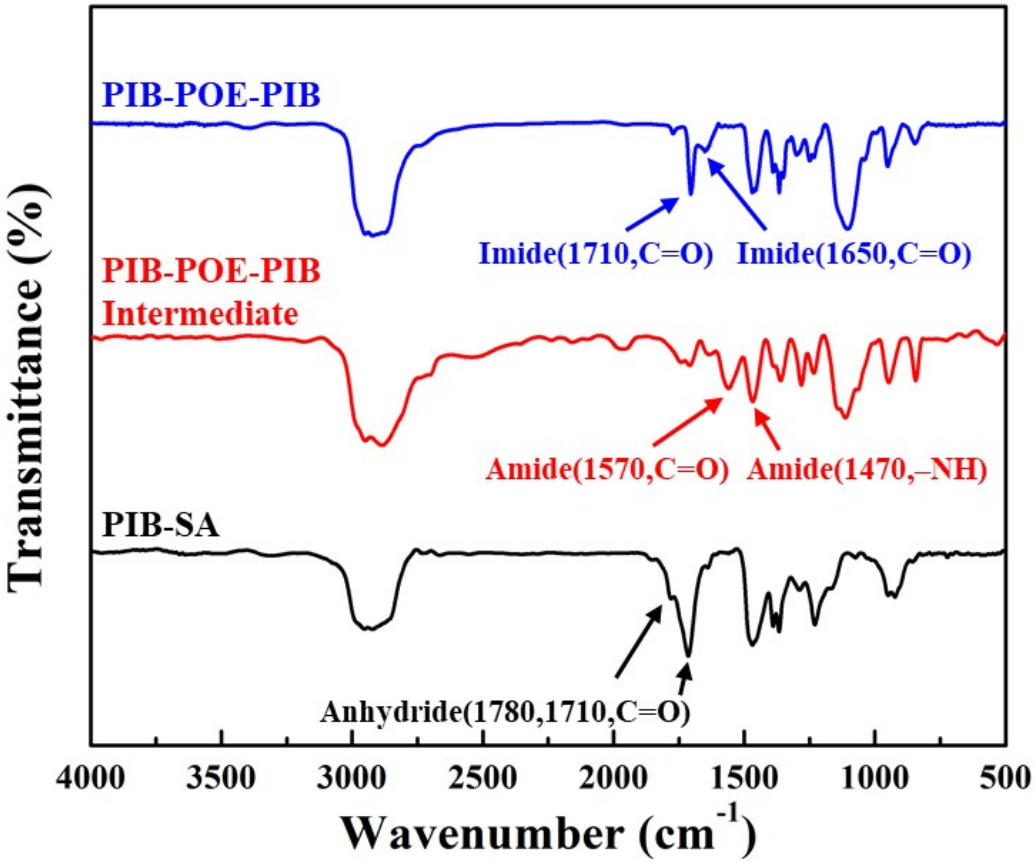

Fig. S6 Fourier transform infrared spectroscopy (FTIR) spectra of PIB-SA, PIB-POE-PIB intermediate, and PIB-POE-PIB. The synthesis of the amphiphilic polymer PIB-POE-PIB was confirmed by the appearance and disappearance of peaks of specific functional groups. For the original anhydride functional group of PIB-SA, anhydride (C=O) stretching-vibration peaks appeared at 1710 cm^{-1} and 1780 cm^{-1}. After the ring-opening reaction with POE2000, the anhydride stretching vibration peaks disappeared, and the resulting amide functional group exhibited a carbon–oxygen double bond at 1470 cm^{-1} and –NH characteristic absorption peak at 1570 cm^{-1}. This was followed by a three-hour ring-closing reaction at 150 °C. At this time, the –NH stretching-vibration peak at 1570 cm^{-1} disappeared, and the main absorption peaks of the imide functional group appeared at 1650 cm^{-1} and 1710 cm^{-1}.

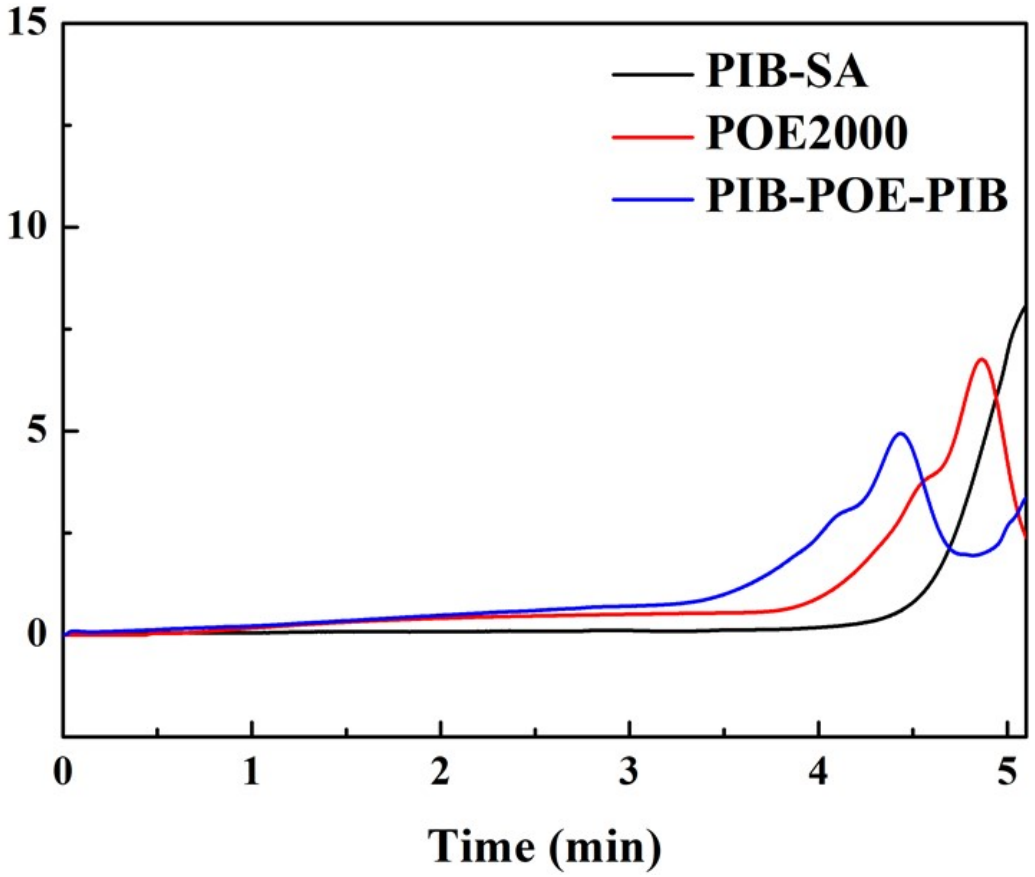

Fig. S7 Gel permeation chromatography (GPC) spectra of PIB-SA, POE2000, and PIB-POE-PIB (a triblock copolymer dispersant). GPC testing was performed using polystyrene as a standard and tetrahydrofuran solvent.

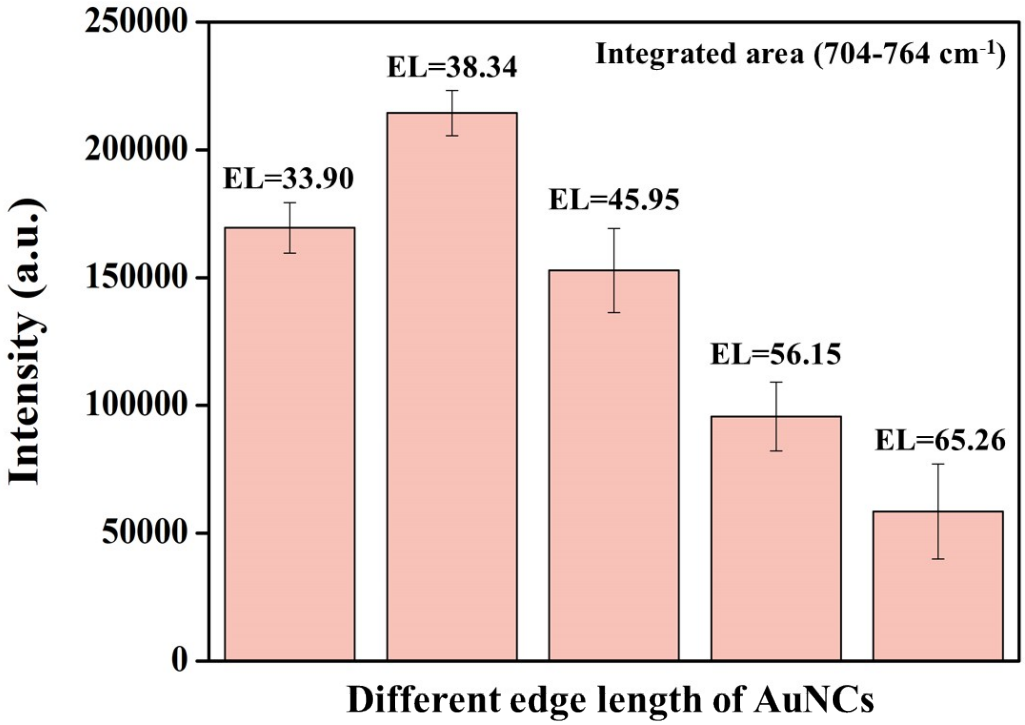

Fig. S8 Comparison of the integrated intensity of SERS signals in the detection of same-concentration adenine (10^{-4} M) using AuNCs of various edge lengths (the wavelength range of the integrated intensity was 704–764 cm^{-1}). AuNCs at 38.34 nm exhibited the best SERS intensity, which was 2.14×10^5.

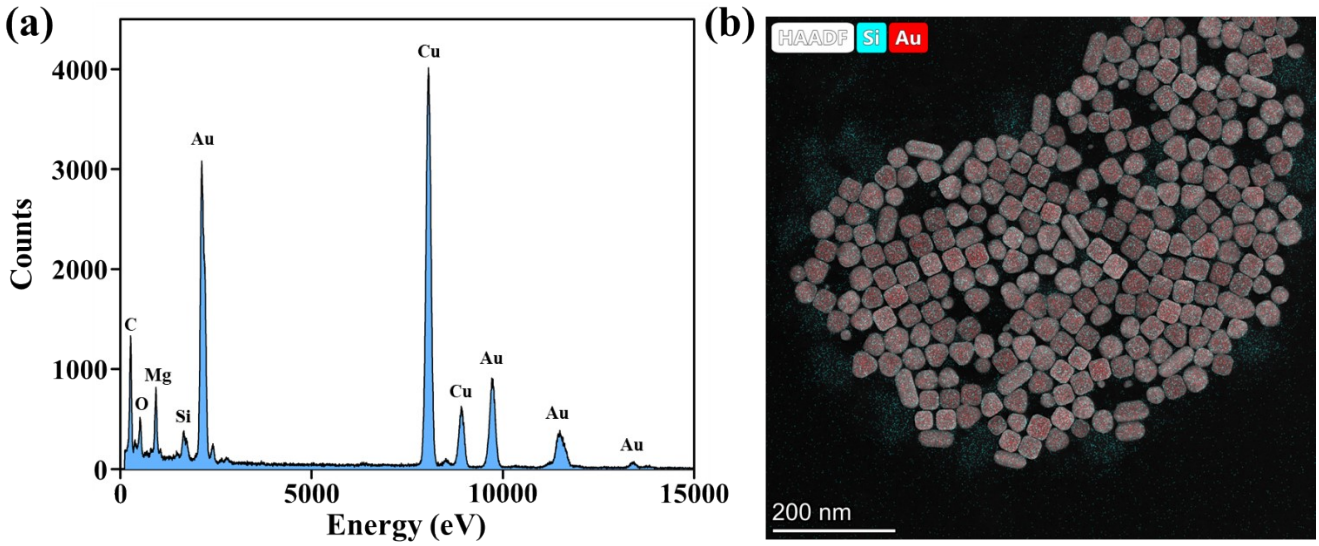

Fig. S9 (a) EDS was used to identify the elemental composition of AuNCs/NMPs, in which Si, O, and Mg were the chemical composition of NMPs. (b) The growth of AuNCs on the surfaces of the NMPs was observed by EDS mapping; the dark red area is Au and the bright cyan area is Si.

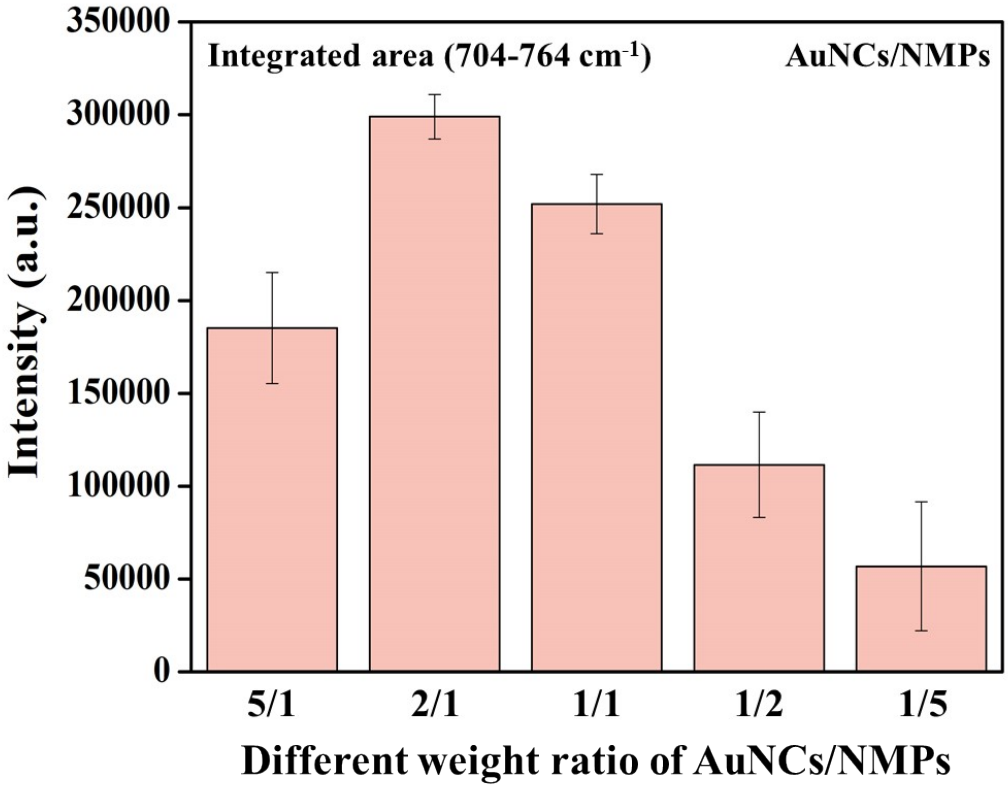

Fig. S10 Comparison of the integrated intensity of SERS signals in the detection of same-concentration adenine (10^{-4} M) using AuNCs/NMPs at different weight ratios (the wavelength range of the integrated intensity was 704–764 cm^{-1}). The SERS intensity of AuNCs/NMPs at a weight ratio of 2/1 reached 3.01 $\times 10^5$.

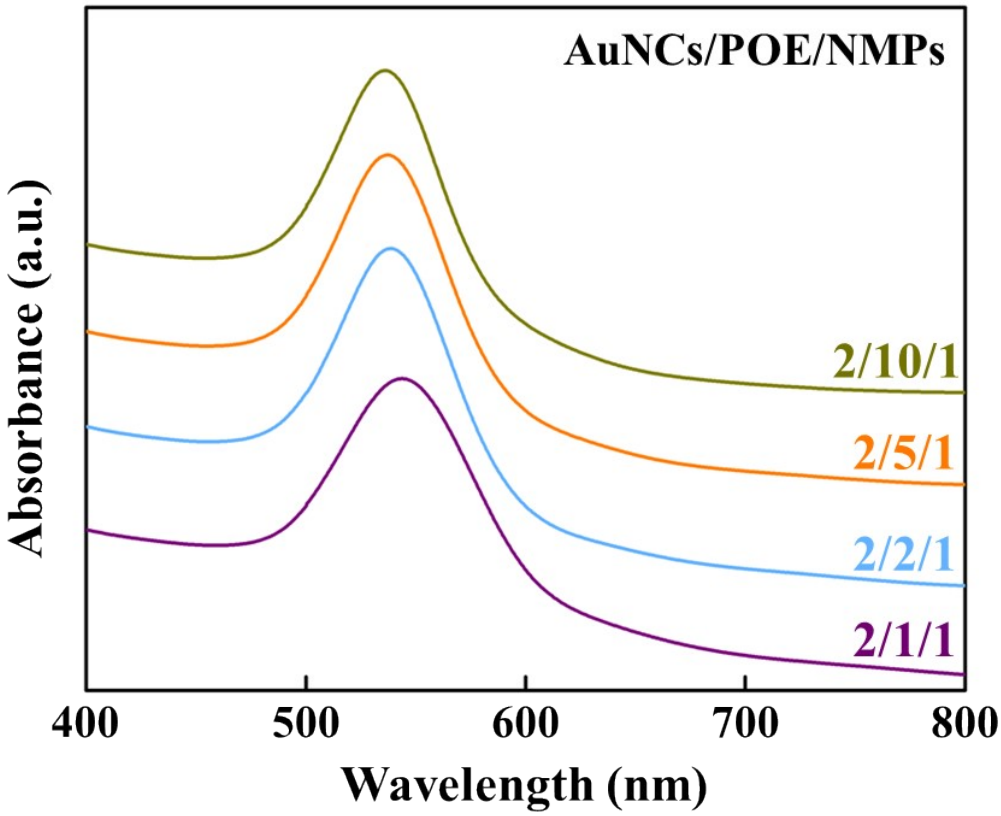

Fig. S11 UV spectra of AuNCs/POE/NMPs-substrate synthesis at different weight ratios.

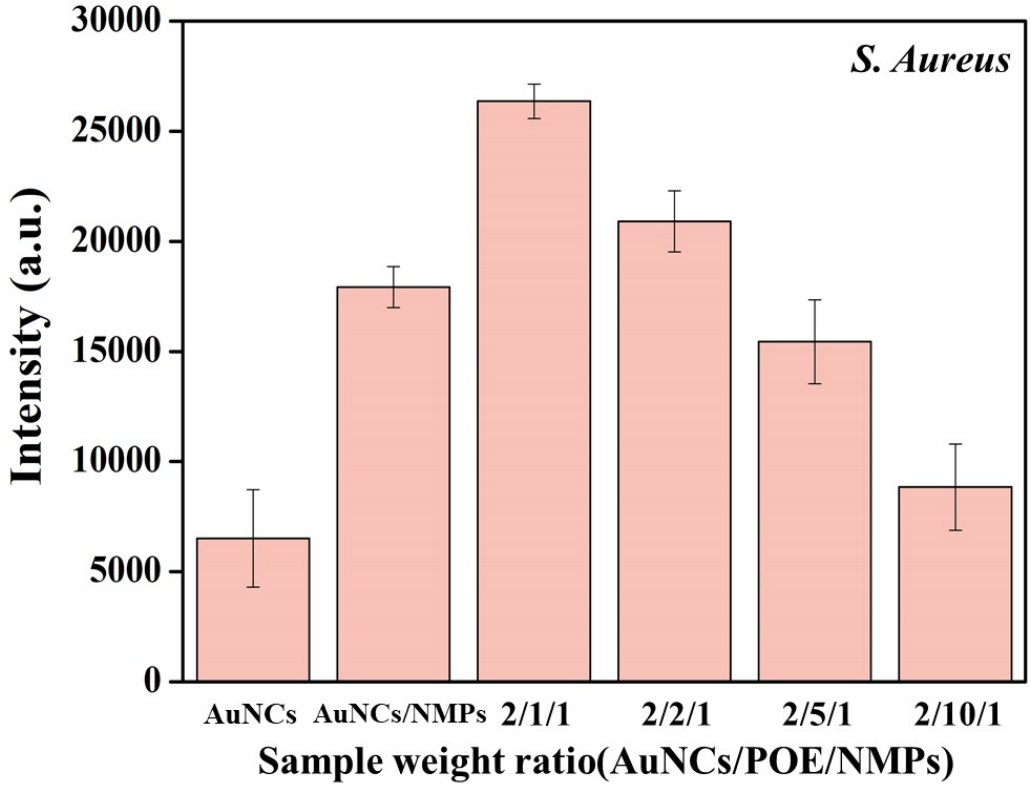

Fig. S12 Comparison of the SERS-signal intensity for the detection of Staphylococcus aureus (10^6 CFU/mL) using AuNCs, AuNCs/NMPs, and AuNCs/POE/NMPs at various weight ratios (the characteristic peak was at 733 cm^{-1}). The SERS intensity reached 2.63×10^4 when the weight ratio of the AuNCs/POE/NMPs was 2/1/1.

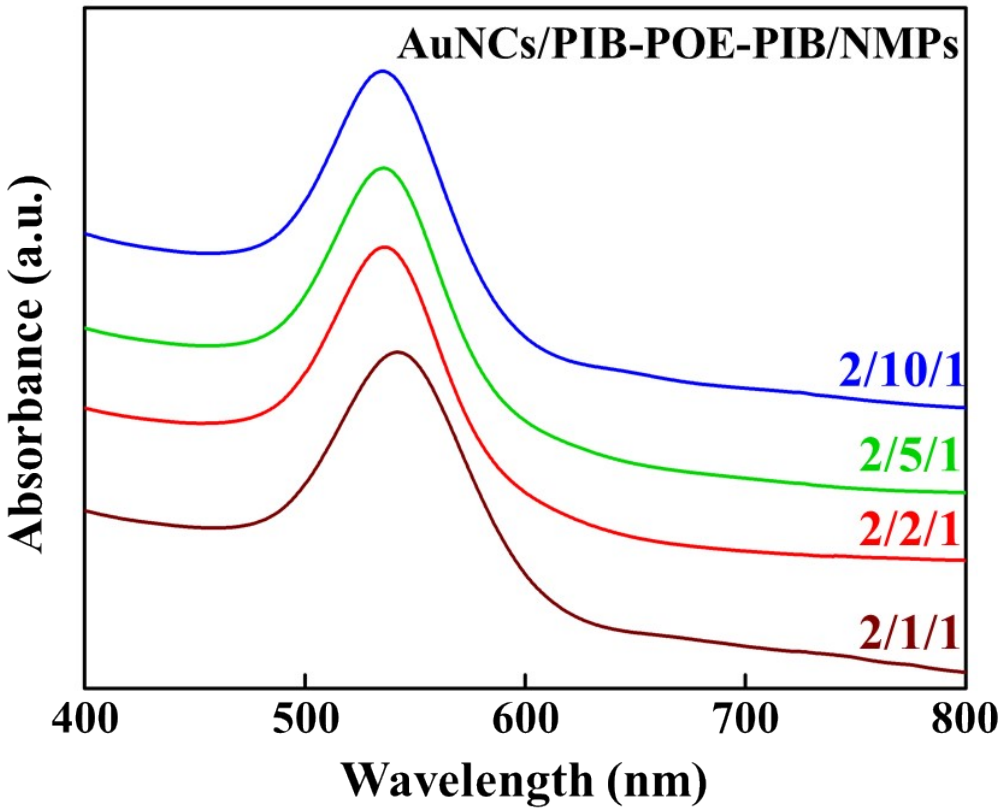

Fig. S13 UV spectra of AuNC/PIB-POE-PIB/NMPs substrate synthesis at different weight ratios.

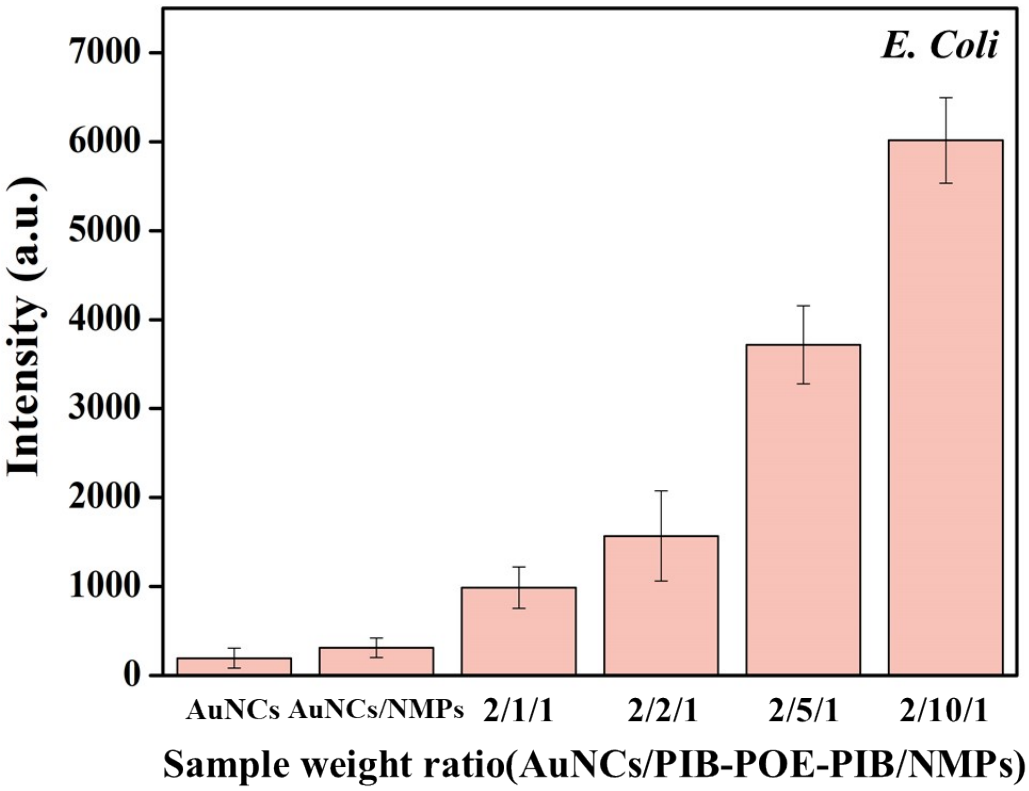

Fig. S14 Comparison of the SERS-signal intensity for the detection of Escherichia coli (10^8 CFU/mL) using AuNCs, AuNCs/NMPs, and AuNCs/PIB–POE–PIB/NMPs at various weight ratios (the characteristic peak was at 730 cm^{-1}). The SERS intensity reached 6.01×10^3 when the weight ratio of AuNCs/PIB-POE-PIB/NMPs was 2/10/1.

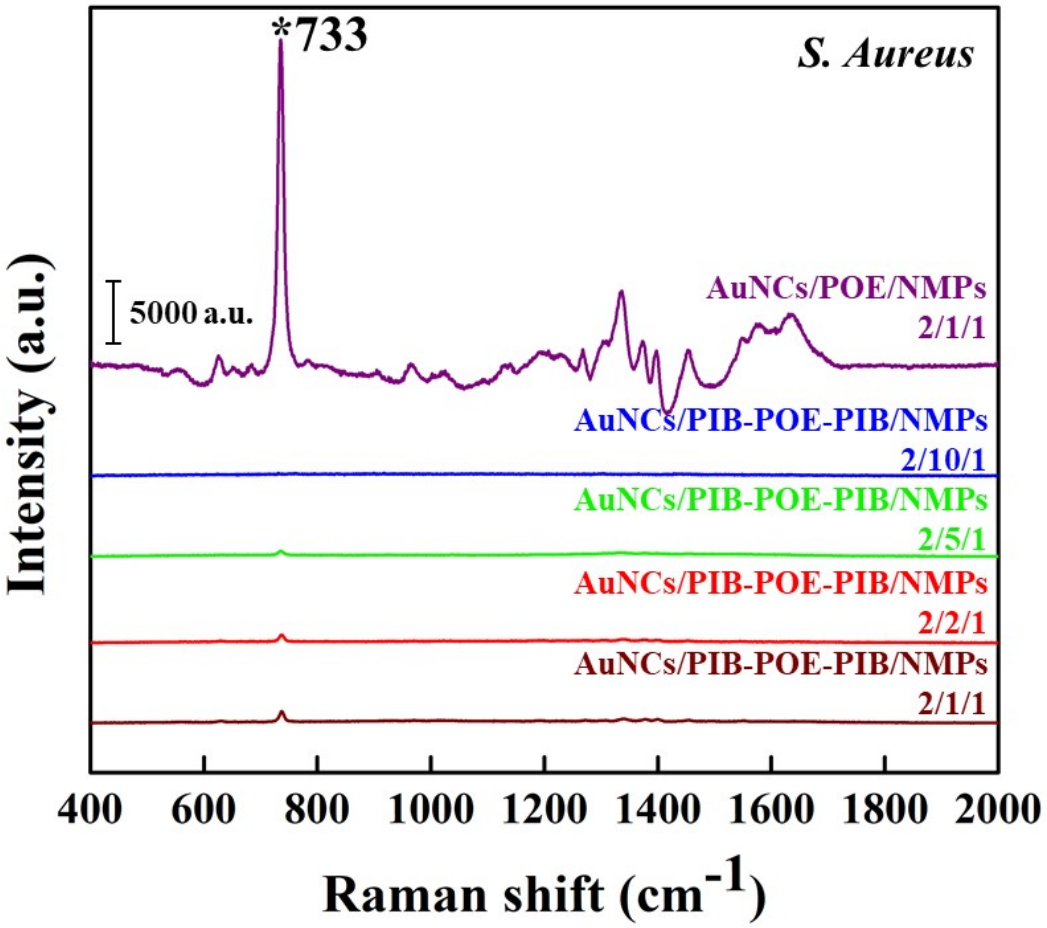

Fig. S15 SERS spectra of Staphylococcus aureus detected using AuNCs/POE/NMPs and AuNCs/PIB-POE-PIB/NMPs at various weight ratios. The SERS signals of Staphylococcus aureus failed to be detected or enhanced using AuNCs/PIB-POE-PIB/NMPs, showing enhanced selectivity of AuNCs/POE/NMPs.

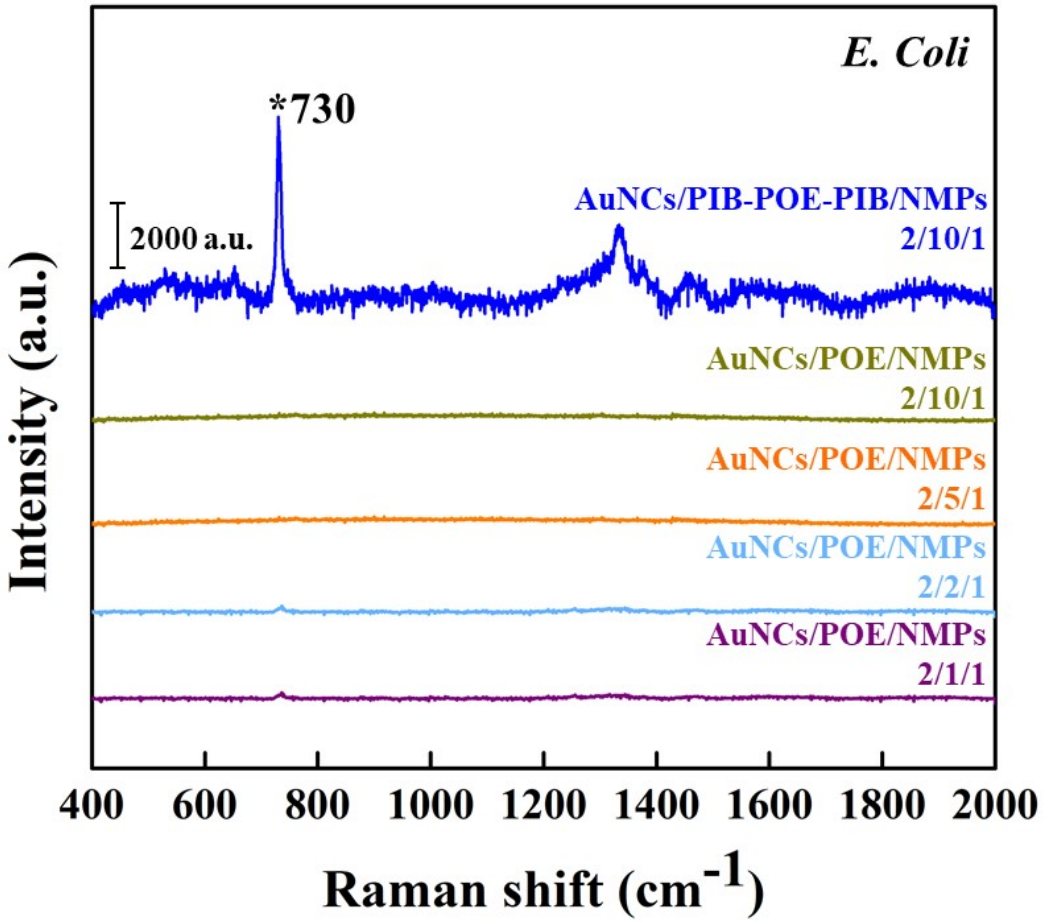

Fig. S16 SERS spectra of Escherichia coli detected using AuNCs/PIB-POE-PIB/NMPs and AuNCs/POE/NMPs at various weight ratios. The SERS signals of Escherichia coli failed to be detected or enhanced using AuNCs/POE/NMPs, showing enhanced selectivity of AuNCs/PIB-POE-PIB/NMPs.

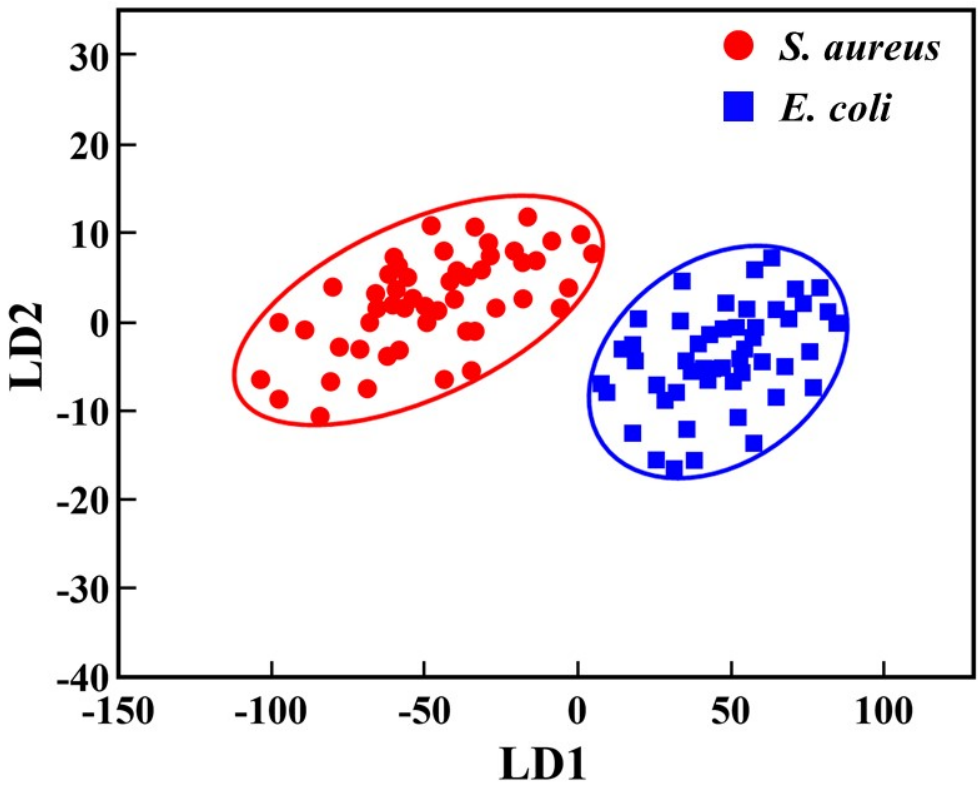

Fig. S17 Combinations of PCA loading profiles of *S. aureus* (red line) and *E. coli* (blue line).

Table S1. Summary of various Au-related nanohybrid substrates for SERS bacterial biosensor.

Hybrid composition[a]	Analyte molecule or bacteria detected	SERS LOD[b]/EF Value[c]	Reference
AuNPs	Adenine	3.5×10^{-8}M/1.0×10^{6}	S1
AuNPs/Silicate		10^{-9}M/Not given	S2
AuNRs/$Ti_3C_2T_x$		10^{-9}M/Not given	S3
TAuNPs/NMPs		10^{-9}M/5.7×10^{7}	S4
AuNCs/NMPs		10^{-9}M/3.6×10^{8}	Our work
AuNPs/PDMS[d]	*Staphylococcus aureus*	13 CFU/mL	S5
M13-AuNPs[e]		10 CFU/mL	S6
Gold nanoflower		10^{3} CFU/mL	S7
AuNCs/POE/NMPs		92 CFU/mL	Our work
Au@AgNR	*Escherichia coli*	10^{2} CFU/mL	S8
AuNRs[f]		8.4 CFU/mL	S9
AuNCs/PIB–POE–PIB/NMPs		1.6×10^{2} CFU/mL	Our work

[a] AuNPs are gold nanoparticles; AuNRs are gold nanorods; TAuNPs are triangular gold nanoplates; Au@AgNR is a gold@silver core-shell nanorod.
[b] Limit of concentration to detect.
[c] An enhancement factor (EF) of SERS activity based on calculations using the following equation: $EF = (I_{SERS} / C_{SERS}) / (I_{norm} / C_{norm})$.
[d] An aptamer (Apt 1) is modified on the substrate through a Au–S bond as the capture probes.
[e] M13 phage with specific *S. aureus*-binding heptapeptide displayed on the N-terminal of pIII protein is selected from phage display peptide library.
[f] The two Au NR-based bioconjugates were functionalized with a suitable antibody (anti-*E. coli* Ab or Ab) that was able to target surface antigens of *E. coli.*

References

S1. J. Zhou, D. Wang, H. Yang and F. Wang, *Spectrochim. Acta A Mol. Biomol. Spectrosc.*, 2022, **270**, 120801.

S2. Y. C. Lee and C. W. Chiu, *Nanomaterials*, 2019, **9**, 324.

S3. P. F. Wu, X. Y. Fan, H. Y. Xi, N. Pan, Z. qian Shi, T. T. You, Y. K. Gao and P. G. Yin, *J. Alloys Compd.* 2022, **920**, 165978.

S4. Y. F. Chen, W. R. Chang, C. J. Lee and C. W. Chiu, *J. Mater. Chem. B,* 2022, **10**, 9974–9983.

S5. A. Zhu, S. Ali, Y. Xu, Q. Ouyang and Q. Chen, *Biosens. Bioelectron.,* 2021, **172**, 112806.

S6. X. Y. Wang, J. Y. Yang, Y. T. Wang, H. C. Zhang, M. L. Chen, T. Yang and J. H. Wang, *Talanta,* 2021, **221**, 121668.

S7. S. Juneja and J. Bhattacharya, *Colloids Surf. B,* 2019, **182**, 110349.

S8. L. Bi, X. Wang, X. Cao, L. Liu, C. Bai, Q. Zheng, J. Choo and L. Chen, *Talanta,* 2020, **220**, 121397.

S9. F. Petronella, D. De Biase, F. Zaccagnini, V. Verrina, S. I. Lim, K. U. Jeong, S. Miglietta, V. Petrozza, V. Scognamiglio, N. P. Godman, D. R. Evans, M. McConney and L. De Sio, *Environ. Sci. Nano,* 2022, **9**, 3343–3360.